Complex seabed geomorphology shaped by various oceanographic processes: a case study from the Gippsland Basin, offshore south-eastern Australia

Nan Wu[1*], Yakufu Niyazi[2], Michael J. Steventon[3], Harya D. Nugraha[4]

[1]State Key Laboratory of Marine Geology, Tongji University, 1239 Siping Road, Shanghai, 200092, China

[2]Minderoo-UWA Deep-Sea Research Centre, School of Biological Sciences and UWA Oceans Institute, The University of Western Australia, Perth, WA 6009, Australia

[3] Shell Research, Shell Centre, London, SE1 7NA, UK

[4] Center for Sustainable Geoscience, Universitas Pertamina, Jakarta, 12220, Indonesia

[*]Email: nanwu@tongji.edu.cn

ABSTRACT

The Gippsland Basin is located in the south-eastern continental margin of Australia and hosts a variety of important marine resources (i.e. hydrocarbons, offshore wind, biological diversity, and fishing resources). Recent high-resolution seabed mapping reveals a complex seabed morphology in the Gippsland Basin, containing scarps, cyclic steps, channels, canyons, gullies, and giant submarine landslides. However, previous studies have not yet revealed the dominant sedimentary processes behind this morphological complexity. We combine high-resolution multibeam bathymetric and seismic reflection datasets to investigate the dominant sedimentary processes that are active in shaping these complex seabed morphologies. In the northern region of the study area, slope failures are prevalent on the shelf and slope, which are primed by the deposition of contourites generated by the East Australian Current. In the central and southern regions, the Bass Cascade Current can carry large amounts of sediments, scouring the shelf and slope, and can form supercritical turbidity currents that create a variety of erosional seabed morphologies. We suggest that slope gradient variation, oceanography and a variety of sedimentary processes jointly contributed to the seabed morphological complexity in the Gippsland Basin. The high-resolution seabed morphological analysis within this study provides critical geomorphological and geological information for future submarine constructions (i.e. locating potential wind farms and telecommunication cable installations) along with geohazard prediction and mitigation (i.e. knowing the location of past and predicting future giant landslides).

Keywords: Gippsland Basin, Seabed morphology, Sedimentary processes, Submarine landslides, Super critical turbidity currents

INTRODUCTION

The Gippsland Basin is one of Australia's most prolific basins for hydrocarbon production, fishing, carbon storage, and other marine resources. At present it is a cool-water carbonate system located on SE Australian's passive margin (Figure 1A; Rahmanian et al., 1990; Mitchell et al., 2007a; Mitchell et al., 2007b). From shelf to slope, the seabed of the Gippsland Basin hosts a variety of seabed morphologies. A number of canyons, channels, gullies, and submarine landslides initiated from the continental shelf edge coalesce on and are captured by the huge Bass Canyon at the lower slope, and ultimately drain SE to the Tasman Abyssal Plain, where water depth ascends over 4000 m (Figure 1C). The complex sedimentary system reflects the action of a range of oceanographic, sedimentological, and tectonic processes at multiple spatiotemporal scales. Despite the morphology complexity, the controls and evolution processes of seabed morphology and sedimentary processes are less well documented in the Gippsland Basin. Therefore, this study aims to address the following questions: (i) Why is seabed morphology so complex in the Gippsland Basin? and (ii) what are the dominant sedimentary processes in the basin?

This study combines bathymetric multibeam and seismic reflection datasets to understand the form and evolution of seabed morphology and sedimentary processes in the Gippsland Basin. First, we aim to delineate the morphological features along the continental shelf and slope areas. Second, we provide an interpretation of the sedimentary processes that are active in shaping these morphological features. Finally, we analyse the effect of oceanographic and sedimentary processes on the development of these sedimentary systems, providing an analogue to other similar submarine settings worldwide.

GEOLOGICAL SETTING

The Gippsland Basin

The Gippsland Basin is Australia's easternmost continental margin basins, located between the mainland of Australia and Tasmania (Figure 1A,1B; Rahmanian et al., 1990). The Gippsland Basin is approximately 400 km long and 80 km wide, with 80% of the basin currently located offshore (Hocking, 1972; Willcox et al., 1992). The Gippsland Basin belongs to a series of rift basins formed along the southern margin of the Australian plate, due to the separation of the Antarctica and Australian continents during the breakup of Gondwana in the Mesozoic (Colwell et al., 1993). The basin is internally divided by four sets of approximately E-W oriented fault systems: the Rosedale and Lake Wellington Fault systems to the north, and the Foster and Darriman Fault systems to the south (Figure 1C; Hegarty et al., 1985). These major fault complexes separate the basin into several structural areas, including the Northern, Central and Southern areas respectively (Figure 1C; Hegarty et al., 1985). The SE margin of the Gippsland Basin is connected by c. 120 km long and 15-70 km wide, ESE-trending Bass Canyon system (Figure 1C). The Bass Canyon has acted as a major conduit and key element in the source-to-sink system in the SE Australian area since the Late Cretaceous (approximately 80 Ma; Hill et al., 1998).

Oceanography and Climate

The Northern region of the Gippsland Basin is influenced by the Eastern Australian Current (EAC; Mitchell et al., 2007b). The EAC meanders south along the east coast of Australia, flowing at a velocity of c. 7.4 km/h (Suthers et al., 2011). The EAC carries warm tropical seawater from the Coral Sea southwards to mix with the cool temperate water of the Tasman Sea (Figure 1A, 1B). The EAC southwards heat transport has increased the intensity and location of storms and wave actions (i.e. eddies), resulting in complex topography along the eastern Australia coastline (Figure 1B; Ridgway and Hill, 2009). The Southern and Central regions of the Gippsland Basin are influenced by the seasonal Bass Cascade Current (BCC) (Figure 1A, 1C; Mitchell et al., 2007b). The BCC was formed due to the cold, denser Bass Strait seawater flowing into and sinking beneath the warmer, fresher water of the Gippsland shelf, generating a northeast flowing current and sinking to the 200 m isobath (Godfrey et al., 1980; Li et al., 2005; Mitchell et al., 2007b). The BCC is a high-energy current with an average transport rate of 3.6 km^3/h (Godfrey et al., 1986). During transportation, the BCC could generate near-bottom gravity flows (dominantly turbidity currents) that transport across the shelf, and downslope over tens and hundreds of kilometres (Ivanov et al., 2004; Wu et al., 2023). In the Central region, the shelf is also dominated by seasonal eastward flowing westerly wind at a speed of 10-30 km/h (especially in winter; Li et al., 2005). The intense westerly wind has created a moderate to high energy wave-dominated environment in the shelf area of the Central region (Figure 1B; Mitchell et al., 2007a; O'Brien et al., 2018).

DATASET

Multibeam bathymetry data for this study is from Geoscience Australia's Marine data portal (http://marine.ga.gov.au). The dataset is compiled from multiple bathymetric surveys and gridded at 50x50 m; hence, geomorphological features smaller than 50 m across cannot be differentiated. The multibeam bathymetry dataset covers the

Gippsland Basin continental shelf, at around 200 m water depth, to the Tasman Sea Abyssal plain, at over 4000 m water depth (Figure 2A&2B). Two types of seismic reflection data are adopted in this study: (i) five 2D regional seismic sections up to c. 1500 km long, therefore providing excellent coverage from the Gippsland Basin shelf region to Bass Canyon abyssal plain (Figure 3A-D, 4B); and (ii) three 3D seismic reflection surveys, including Elver 3D, Tuskfish 3D, and Oscar 3D (reprocessed in 2012), which cover an area of c. 650 km^2, 1050 km^2, and 1200 km^2, respectively (Table 1, Figure 2B). The 3D seismic datasets are zero-phase; with a SEG normal polarity where a downward decrease and increase in acoustic impedance are expressed as blue (negative) and red (positive) seismic reflections, respectively. We calculate an approximate vertical resolution of c. 10-12.5 m for the near seabed sediments, using the dominant frequency content of 40/50 hertz and an average seismic velocity of 1700 m/s for the near seabed sediment.

RESULTS

Northern region

The Northern region spans 120 km long and 90 km wide (Figure 2B, 4A). In the regional seismic sections, the continental shelf area has a gently dipping (<1^o) seabed with an average water depth of 110–150 m (Figure 3A, 3B). Based on the slope gradient, we subdivide the Northern region into the eastern and western parts (Figure 4A). In the eastern part, the shelf break marks a gradual transition from a shallow-dipping (0.75^o) shelf to a relatively steep (2.27^o) slope, at approximately 1500 m water depth (Figure

3A). In the western part, the shelf break marks a distinct transition from the shallow-dipping shelf (0.08°) to a steep dipping slope (7.82°) at approximately 1000 m water depth (Figure 3B). In the following part, we describe the morphological features and interpret their associated sedimentary processes from the continental shelf to the slope area.

Observation: In the eastern part, extensively distributed giant scarps are observed near the shelf edge and on the slope, where a single scarp can reach more than c. 30 km wide (Figure 4A). At least two submarine landslides (landslide-1 and landslide-2) are observed on the slope. These landslides are scalloped shaped, occurring on the seabed gradient of c. 20°. They are prodigious in scale, and each landslide extends for at least 25 km wide and 40 km long, involving an area of c. 700 km^2 (Figure 4A). Within these landslides, a series of scallop-shaped internal scarps that form a terraced pattern are observed (Figure 4A). In the seismic section, the scarps are nested in a stair-like style, showing a truncated reflector that cuts through upslope strata (Figure 4B).

A shelf-indented canyon (Everard Canyon) is found in the middle part of the Northern shelf (Figure 4A). The head of Everard Canyon is c. 40 km upslope to the shelf break, initiating at a water depth of 200 m and extending to the lower slope where the water depth is more than 3500 m (Figures 2A&4A). The canyon head is characterised by a dendritic shape, comprising a major branch and two deep landward excavated tributaries (Figure 4A). The upper section of Everard Canyon initially follows the dip direction of the continental shelf, then alters its direction to NE-SW when it debouches to the edge of the shelf. Terrace-shaped scarps are evident above the eastern canyon sidewall but less pronounced above the western sidewall (Figure 4A). In a cross-sectional view, Everard Canyon is characterised by U-shaped geometry, with steep sidewalls (c. 30°) and relief of c. 600 m (Figure 4B). Additionally, no seismically visible deposition is observed on the canyon floor (Figure 4B). On the lower slope, Everard Canyon contains multiple scarps (Figure 4A). In a dip-sectional profile cut along Everard Canyon, these scarps are characterised by an upslope stair-shaped geometry (Figure 4C). NW to Everard Canyon, three slope-confined canyons (Shark, Sole and Whaleshark Canyons) originate from the northern meander plain and intersect Bass Canyon at their lower end (Figure 4A). These slope-confined canyons dissipate above the middle slope to a point canyon head and are characterised by a U-shaped cross-sectional geometry (Figure 4D).

In the western part of the Northern region, numerous failure scarps are evident on the continental shelf where the slope gradient is $<1^{\circ}$ (Figure 5A). Generally, these scarps dip from east to west, with widths ranging from c. 5 km to 20 km. In seismic sections, these scarps show a stair-shaped, backward (i.e. landward) dipping geometry. Beneath the seabed, a series of sub-parallel to wavy, alternating medium to high amplitude, internal truncated seismic reflections with channel-shaped external forms are identified in the seismic sections (Figures 5B, 5C). Parallel and continuous reflections with mounded external forms are adjacent to the channel-shaped seismic packages

(Figures 5B, 5C). Several sub-parallel to wavy seismic reflections with channel-shaped external forms lie beneath the seabed (Figures 5B and 5C). Parallel, continuous seismic reflections with mounded external forms are immediately adjacent to the channel-shaped seismic reflections. Further downslope, widespread seabed gullies are oriented perpendicular to the local slope contours and dip toward south and southeast in the slope area (Figure 4A). The gullies originated from the northern shelf edge and fed into the eastern boundary of Bass Canyon. They are characterised by a set of straight, closely spaced (130-280 m), sub-parallel and channel-shaped features. In cross-section, gullies are V-shaped and steep-sided, with a relief (incision depth) of 40-170 m and a width of 300-500 m (Figure 4E).

Interpretation: The presence of the stair-stepped scarps in the eastern part indicates that the landslides are initiated on the lower slope and fail retrogressively upwards (i.e. Sawyer et al., 2009; Wu et al., 2022). In the western part, the scattered scarps on the shelf suggest that slope failures dominate the continental shelf area. The water depth of the shelf is between 200-500 m, where cyclic wave loading can constantly rework seabed sediments and account for the potential trigger mechanism that results in slope failure (i.e. Marshall et al., 1978; Bea et al., 1983). Further downslope, the dip direction of gullies is sub-perpendicular to the strike direction of the scarps. This close proximity of the scarps and gullies indicates the latter originated from slope failures (i.e. Gardner et al., 1999; Gales et al., 2012). The repetitive slope failures occurring on the shelf are likely to generate stable debris flow and turbidity current that is continuously transported downslope, which erode the seabed and lead to gullies' initiation (i.e. Micallef and Mountjoy, 2011; Lonergan et al., 2013).

The seismic expressions of channel-shaped seismic packages are similar to those of buried contourite channels (Faugères et al., 1999; Stow et al., 2002), and the mounded seismic packages are buried contourite drifts (Figures 5B, 5C; Miramontes et al., 2021). The deposition of the buried contourites is attributed to the presence of the along-slope current, we infer that the along-slope current flow towards the SW-WSW, as the current direction is generally perpendicular (Flood, 1988) or oblique (Blumsack and Weatherly, 1989) to contourite channel crests. As the EAC is the major current that operates in this region with flowing to SW, we infer the EAC is most probably responsible for the formation of the buried contourite channels and drifts. The deposition of the buried contourites indicates that the shelf has a high sedimentation rate (i.e. Howe et al., 1994), therefore, is vulnerable to slope failure (Laberg and Camerlenghi, 2008; Miramontes et al., 2018).

Everard Canyon is the largest tributary to Bass Canyon (Figure 2B). It has not connected with any fluvial system, meaning that there is limited terrestrial input from landward (Mitchell et al., 2007b). The alongshore movement of EAC has consistently transported sediments into the head area of Everard Canyon (Mitchell et al., 2007b). Our observations suggest that the SW propagating EAC would heavily impinge the eastern canyon sidewall, causing slope failures and abundant scarps. The absence of seismically visible intra-canyon infills suggests that the heads of Everard Canyon were flushed by presently active erosional processes. We interpret that the most likely erosional process is gravity flows generated by canyon sidewall failures (i.e. Wu et al., 2021). The shift in the canyon transportation direction from SE to SW is primarily controlled by the local topography created by the regional Rosedale Fault (Figure 1C). The stair-shaped scarps developed within Everard Canyon near the lower slope indicate long-term retrogressive failures that have occurred over time (Sawyer et al., 2009). This may suggest that canyons in the Northern region are most likely to be originated from the lower slope and migrate retrogressively through slope failure processes (Farre et al., 1983; He et al., 2014).

Central region

The continental shelf of the Central region extends seaward for approximately 70 km at an average dip of 0.8° then abruptly steepens to an average dip of 8.8° reaching the slope area (Figure 2B, 3C). The Central region has the steepest continental slope within the study area. Our observations suggest this region is dictated by a different oceanographic and sedimentary processes relative to the Northern region.

Observation: On the shelf, multibeam and 3D seismic datasets document a c. 40 km long scarp that separates the undeformed shelf from a set of erosional features (Figure 6A). Seismic sections cutting through the scarp reveal that well-layered, undeformed strata are separated by moderately deformed, discontinuous strata, bounding by a continuous base surface (Figure 6B). East to the scarp, a series of regularly spaced oval and crescent-shaped bedforms are observed near the SE part of the shelf (Figure 6A). In the seismic section, the oval-shaped bedforms are scour-like undulations that are repeated at regular intervals (c. 0.6-2 km). A single bedform is characterised by a truncated, gently lee side and short, steep stoss sides (Figure 6B). The crescent-shaped bedforms are aligned in-train and gradually formed as a channel-shaped morphology (Figure 6A). In the seismic section, a single crescent-shaped bedform is characterised by a steep lee side and a gently dipping stoss side (Figure 6C). The crescent-shaped bedform train has a broad bowl-shaped morphology that lies above an erosional base surface (Figure 6D).

Further north of the shelf, at least two well-developed channels are observed near the northern part of the shelf (Figure 6A). These channels initiate from the outer shelf and extend to the shelf break (Figure 6A). They display trough-shaped depressions with a flat base surface in the seismic cross-section (Figure 6D). On the slope, widely distributed and predominant gullies extending from the shelf edge to and intersecting with the Bass Canyon head are observed (Figure 6A). The gullies are characterised by straight and linear morphology, dipping parallel to the slope dip direction. The cross sections show the gullies are V-shaped, and have a clear erosive truncation along the sidewalls (Figure 6D).

Interpretation: Wu et al. (2023) have thoroughly investigated the initiation and evolution of these seabed morphologies and dominant sedimentary processes in the Central region. It was suggest that the complex seabed morphology in this region is genetically linked to a dynamic interaction between Bass Cascade Current, Westerly wind, and strong waves (Wu et al., 2023). The NNE-trending scarp developed on the shelf is interpreted as the headwall scarp of larger buried submarine landslides (i.e. Bull et al., 2009). The oval- and crescent-shaped bedforms are likely cyclic scours (i.e. Fildani and Normark, 2004; Kostic, 2011) and cyclic steps (i.e. Fildani et al., 2006), respectively. These bedforms are formed by downslope flowing of supercritical currents while excavating the seabed through the force of hydraulic jumps (Gardner et al., 2020). The intermediate relation of these bedforms to the gully heads suggests that erosion by the overflow of supercritical turbidity currents could play a significant role in the initiation of gully formation (i.e. Noormets et al., 2009; Gales et al., 2012). Based on Wu et al. (2023) the headwall scarp developed on the shelf could catch the along-shelf transported BCC, forcing it to sink and generate supercritical turbidity currents. The supercritical turbidity currents further transports downslope, forming the widely distributed gullies and other erosional structures on the slope. The Westerly winds and associated waves could also impact the area off-shelf and across the upper slope, forming submarine landslides and initiating turbidity current (Wu et al., 2023).

Southern region

The Southern Region is c. 70 km long and c. 120 km wide (Figure 2B). In the regional seismic section, the continental shelf area has a gently dipping (1.12°) seabed, and the continental slope marks a gradual transition from a steep-dipping (5.37°) upper slope to a gradual dipping (1.61°) lower slope, at approximately 3000 m water depth (Figure 3D).

Observation: In the Southern Region, five shelf-indenting canyons extending from the continental slope towards downslope to converge with the Bass Canyon are observed (from north to south: Anemone, Archer, Pisces, Moray and Mudskipper canyons; Figure 7A). Dendritic heads are characteristic of all canyons except the Archer Canyon. The Anemone Canyon head is strongly asymmetrical and has three deeply incised channels in its head area (Figure 7A). Canyons in the Southern region are evenly spaced (c. 11-14 km), flowing from E to SE and oriented along the slope dip. On the upper slope, the canyons display channel-like nature and show linear geometry with no bifurcation (Figure 7A). On the middle slope, canyon geometry changes from linear to meander and then shifts to bifurcate or even braid farther downslope, where the slope gradient is minor. On the lower slope, canyons alter to sinuous stream-like features and gradually loses expression and merges into the Bass Canyon (Figure 7A). Throughout the course, canyons maintain a narrow, scour-deep, symmetric cross-sectional geometry with a V-shaped profile (Figures 7B-7D). In the upper part of these canyons, the sidewalls of the canyon are typically steep, with occasional and localised failures occurring along the headwalls and sidewalls (Figures 7A-C).

The seabed of the Southern region is fairly featureless compared to the Northern and

Central regions, where gullies and mass failures are widely distributed (Figure 7A). On the Southern shelf, several sets of crescent-shaped bedforms that are aligned in-train have been imaged near the shelf breaks, often close to the canyon heads (Figure 8A). In cross-section, the crescent-shaped bedforms are morphologically asymmetric, with a steep scarp on the lee side and a gentle dipping slope on the stoss side (Figure 8B). These bedforms are 600-1000 m in wavelength (crest to crest wavelength) and c. 30-60 m in wave height. The overall wavelength and height gradually decrease with water depth (Figure 8C). Further downslope, straight and chute-like upper slope gullies separated by distinct ridges are observed between Archer Canyon and Pisces Canyon at a depth of 1000-1500 m (Figure 8A). These gullies have a limited distribution compared to the gullies developed on the Northern and Central slopes. They are V-shaped and steep-sided in cross-section, with a relief (incision depth) of 100-120 m and a width of 800-1500 m (Figure 8C). Neither landslides nor scarps are evident around or directly upslope the gullies (Figure 8A).

SE to the gullies, widely distributed crescent-shaped bedforms are observed in the upper-middle slope area (Figure 8A). A pattern of these bedforms can be observed in the intra-canyon areas until the lower slope, where they remain prominent (Figure 9A). The crescent-shaped bedforms range from 150-300 m in width, 900-1100 m in length and 70-125 m in depth. Like their counterparts that developed on the shelf, they feature steep lee sides and gentle stoss sides (Figures 8D, 9B). In the upper slope, crescent-shaped bedforms exhibit a distinct pattern of lateral transformation.

Crescent-shaped bedforms convert into an incipient channel shaped morphology, and eventually into a mature channel shaped pattern along the slope strike direction (Figure 8A). On the middle slope, where the slope gradient is less than 2^{o}, extensive scarps are observed along the canyon sidewalls (Figure 9A). These scarps have formed a block-shaped zone that is located along the canyon sidewalls, showing a clear escarpment in the bathymetry cross-section (Figure 9C).

Interpretation: On the shelf, the dendritic-shaped canyon heads indicate canyons are in the juvenile stage in canyon development (Mitchell et al., 2007b). Canyon heads entraining shelf sediments can constantly fuel erosive gravity flows that are transported downslope along the canyon floor (Mitchell et al., 2007b). This explains why canyons developed in the Southern region are featured with V-shaped canyon profiles. Once the canyon heads stabilised, shelf-derived erosive gravity flows will reduce, the canyon cross-sectional profile will switch from V- to U-shaped, and the canyon will develop into a mature stage (Mitchell et al., 2007b). Further downslope, the deflected canyon geometry is interpreted to be caused by the path of canyons shifting over time, leaving the abandoned canyon geometry near the middle- to lower-slope (Hill et al., 1998). Near the lower slope, the block-shaped zone along the canyon sidewall is representative of erosional features caused by repetitive canyon sidewall failures (i.e. Yin et al., 2019). Canyon sidewalls can continue to steepen and destabilize, resulting in local failures and generating turbidity currents, and steeping canyon sidewall gradients (Puga-Bernabéu et al., 2013). We suggest that the continuation of this erosional process can provide local sediment input to the canyon and maintain its propagation into the Bass Canyon, as numerous channel-like features are identified on the Bass Canyon floor, suggesting that Southern slope canyons are active, constantly transporting sediments into deep marines (Figures 2A&2B).

The crescent-shaped bedforms are interpreted as cyclic steps that are usually caused by supercritical turbidity currents during excavation of the seabed through the force of hydraulic jumps (Fildani et al., 2006; Zhong et al., 2015). The intimacy of the cyclic steps developed on the shelf and the canyon heads indicates that supercritical turbidity currents are active in modifying the canyon heads and providing sediment sources for the canyon systems (Paull et al., 2002; Post et al., 2022). A continuous presence from cyclic steps to gullies, may indicate that the shelf and upper slope areas are continuously shaped and remoulded by the supercritical turbidity current. The widespread distribution of cyclic steps throughout the inter-canyon floor demonstrates the continuing role of supercritical turbidity currents in shaping the seabed. The initiation of the supercritical turbidity currents is interpreted as the volume of the intra-canyon downslope flowing currents being too large, and the canyons cannot accommodate it, thus escaping the canyons and sweeping onto their floors. Under the continuous erosion of the supercritical turbidity currents, the cyclic steps can evolve into a cyclic step train, and the incipient channels, eventually forming the well-developed channels (i.e. Fildani and Normark, 2004; Fildani et al., 2013).

DISCUSSION

Northern region: slope failure dominated area

The presence of widely distributed submarine landslide headwall scarps indicates that slope failures frequently occur on the Northern shelf. Although these landslides have a small area and volume, they may produce erosive gravity flows capable of damaging seabed infrastructure (i.e. wind farms, telecommunication cables, and submarine pipelines; Hsu et al., 2009; Carter et al., 2014). In terms of scale, the landslides mapped on the shelf are comparable with other tsunamigenic landslides (i.e. Parsons et al., 2014). As historical tsunamis have been identified along the Northern shelf since the Late Pleistocene (Bryant and Price, 1997), it is reasonable to predict that this area has higher probability of tsunami generation.

On the Northern shelf, the thick accumulation of contourites may have played a role in the preconditioning of the landslides (i.e. Brackenridge et al., 2020). The contourites are generally fine-grained, poorly sorted, and have low permeabilities (Miramontes et al., 2016; De Castro et al., 2020). Rapid deposition of such sediments favours the generation of excess pore pressure and weak layers that can ultimately trigger slope failures (Solheim et al., 2005; Gatter et al., 2020; Nicholson et al., 2020). In addition, the deposition of contourite drifts can create a set of local high-gradient slopes that can serve as slope failure susceptible structures, which increases slope instability and lead to an increased likelihood of slope failures (Bryn et al., 2005; Rashid et al., 2017; Miramontes et al., 2018).

The intense storms and wave actions created by the EAC along the Australian coastline could also prime and trigger slope failures. Although the sedimentation rate is low along the eastern Australian margin due to a combination of factors such as low mainland sediment flux, limited accommodation space, and longshore drift is generally assumed to have greater effect on sediment transport of the shelf sediments (Short and Trenaman 1992; Keene et al. 2008), recent studies showed that the EAC has a more significant effect on upper and mid-slope margin sedimentation than previously thought (Keene et al., 2008). In addition, the EAC flows southward as the EAC Extension, along the east side of Bass Strait, reaching the east coast of Tasmania (e.g., Ridgway and Dunn, 2003), and the eddies associated with the EAC are up to 200-300 km in diameter, often 2-3 times annually, with a lifetime spanning more than a year (Figure 1B; Boland and Church, 1981). These large-scale eddies follow a complex southward trajectory and are generally constrained within slope settings (Boland and Church, 1981; Ridgway and Hill, 2009). Therefore, eddies and cyclic wave loading can continuously destabilise seabed sediments and ultimately trigger variously scaled slope failures (i.e. Marshall et al., 1978; Bea et al., 1983). Therefore, it is reasonable to presume that the Northern region has a high hazard potential, representing a natural hazard region in the Gippsland Basin. New geological and geophysical datasets (including sedimentary cores, grabbing or dredging samples, additional high resolution sub-bottom profiles, 3D seismic reflection data, crewed submersible dives, and Underwater Autonomous Vehicles) are needed to assess modern seabed conditions (oceanographic and geomorphology) and to provide better suggestions for future geohazard assessments.

Southern and Central regions: the supercritical turbidity currents dominated area

In the Southern region, the evenly spaced nature and the absence of onshore fluvial systems indicate the canyoning process in the Southern region is fully marine and is related to alongshore current activities (Krassay et al., 2004; Mitchell et al., 2007b; Wu et al., 2022). Previous studies indicate the initiation and development of the canyons are attributed to the strengthening of the Bass Cascade Current (BCC) since the Pliocene (Mitchell et al., 2007a). Specifically, the BCC could carry a large amount of sediment and redeposit them on the southern shelf (Mitchell et al., 2007b). This process could increase the sedimentation rate on the shelf and generate downslope-eroding turbidity currents (Mitchell et al., 2007b). Once the turbidity currents are initiated, the canyon heads often play as the major conduits for such currents (Canals et al., 2009; Morrison et al., 2020). It is because of the continuous erosion caused by the turbidity current that modern canyons exhibit extreme erosional canyon heads. Observations of cyclic steps on the shelf and slope suggest that ambient turbidity currents are linked to supercritical turbidity currents (i.e. Fildani et al., 2006; Zhong et al., 2015). The supercritical turbidity currents are continuously shaping and remoulding the shelf and slope areas as evidenced by widely distributed cyclic steps (i.e. Fildani et al., 2013). In the Southern region, it is the along shelf edge transported BCC that dictates shelf morphology and sedimentation. The BCC-initiated supercritical turbidity currents that transport downslope dominate morphology and sedimentary processes in the slope area.

The Central region also receives the seasonal arrival of the Bass Cascading Current (BCC), along and across the continental shelf area (Mitchell et al., 2007b). The BCC can work with pre-existing seabed scarps caused by submarine landslides and initiate supercritical turbidity currents that travel from the shelf and reach the lower slope (Wu et.al 2023). Furthermore, Westerly wind-associated Ekman transport flow and strong waves have also affected the morphology and sedimentary processes of the Central region. Therefore, supercritical turbidity currents dominate sedimentary processes in the Central region. Comparing to the Northern region, the influence of the EAC decreases significantly. A major proportion of the EAC separates from the coast at the north of Sydney, and continues either towards New Zealand (Godfrey et al., 1980), leaving the EAC eddies as one of the dominant oceanic inputs off northeast Tasmania during the summer season (Cresswell and Legeckis, 1986). However, the eddies are generally constrained within slope settings, and reach their the maximum intensity between 30 and 35°S, and therefore, do not have strong influence on the Central and southern region of the study area (Oke et al., 2019).

What dictates the complexed seabed morphology in Gippsland Basin?

The canyons developed in the Northern region are profoundly different from those developed in the Southern region, in terms of their shape, scale and distribution (e.g., Figures 4A, 7A). More specifically, the canyons in the Northern region are generally less incised (c. 50-100 m deep), and slope gradients are relatively flat (less than 10º). In contrast, canyons developed in the Southern region often have more tributaries with higher incision depths (more than 600 m) and steeper slope gradients (more than 35º). These differences might reflect different sedimentary processes, though the two regions are only c. 40 km apart (Figures 2A, 4B).

In the Northern region, the slope-confined canyons (i.e. Sole and Shack canyons) are located on the lower slope (Figure 4A). They are considered to evolve primarily through local slope failures and progressively migrate upslope via retrogressive slope failures (i.e. Farre et al., 1983; Jobe et al., 2011). The canyoning process originated from slope failures initially occurring near the lower slope, further enlarged through intra-canyon retrogressive failure and canyon sidewall collapses, extending upslope direction and ultimately reaching the shelf edge (see the similar process from He et al., 2014). Therefore, the primary mechanisms for canyon initiation and evolution are tied to retrogressive slope failures, which start at the lower slope (Figure 10A; i.e. Pratson and Coakley, 1996; He et al., 2014). In the Southern region, evidence for submarine landslides is only present within the deeply incised dendritic canyon heads (i.e. Figure 7A). Therefore, the slope failures might become important in the canyon development, but they have limited contribution to the canyon initiation. On the Southern slope, the presence of cyclic steps, cyclic step train and channels may represent a channel evolution process (Figure 8A; i.e. Fildani and Normark, 2004; Fildani et al., 2013). The cyclic steps represent morphodynamical signals of the incipient, early incision stage of a channel (Fildani et al., 2013). With the repetitive flushing of the supercritical turbidity currents, the cyclic scours and cyclic steps could develop into gullies or incipient channels and ultimately evolve into canyons (as we observed from the upper slope; 8A). Therefore, in the Southern region, the primary mechanisms for canyon initiation are linked to the downslope erosional process caused by supercritical turbidity currents (Figure 10B; Fildani et al., 2013).

Other factors, such as slope gradients, could also influence seabed morphology. For example, the canyons are linear in the Northern region, where the seafloor gradient is relatively high, and no bifurcation nor diversion is observed (Figure 4A). While in the Southern region, when canyons run into the low gradient lower slope (~ 1^{o}), canyons initiate to meander and bifurcate (Figure 9A). The lower slope gradient in the Southern region also explains why gullies are intensively distributed on the Northern and Central slopes but are less abundant on the Southern slope. This is because the threshold of slope gradient for initiation of gullies is above 5.5° (Micallef and Mountjoy, 2011), while the Southern slope only has an average slope gradient of 5.37^{o}. The lower slope gradient can limit the ability of turbidity currents to decelerate and form hydraulic slams, which in turn allows for cyclic step formation on the Southern slope (Fildani et al., 2006; Normark et al., 2009; Zhong et al., 2015).

Our results suggest that oceanography directly influences sedimentary processes, thus controlling the morphology of seabed. For example, in the Central and Southern regions, the along-shelf edge transported BCC has generated downslope flowing supercritical turbidity currents that have caused erosion in the shelf and slope areas. Due to the presence of prevailing BCC, erosional features related to morphology, such as channels, gullies, and canyons, dominate these areas. In the Northern region, the prevalence East Australian Current has created a slope failure prone environment, making widely distributed scarps and giant landslides are the major morphology in the Northern region. Tectonics could also influence seabed morphology. The presence of the Lake Wellington Fault system in the Northern region has influenced the seabed topography and local gradients, which may cause the direction of Edvard Canyon to change from SE to SW.

CONCLUSION

We combine high-resolution bathymetrical, and 2D and 3D seismic reflection datasets to investigate the seabed morphology and sedimentary processes in the Gippsland Basin, SE Australia. Our results show that:

1. East Australian Current influences the Northern region, causing slope failures and landslides-rich morphologies.
2. The Bass Cascade Current can initiate supercritical turbidity currents that cause cyclic steps, channels, gullies and canyons morphologies, significantly influencing the sedimentary processes in the Central and Southern regions.
3. We indicate that oceanography, sedimentary evolution processes, seabed

gradients, and tectonics have jointly contributed to the complexity of the seabed morphology in the Gippsland Basin.

4. Our study provides new insights into process interactions that influence seabed sedimentation and morphology, which are particularly pertinent to submarine constructions, geohazard mitigations and can be used for paleo-reconstruction interpretations.

ACKNOWLEDGMENTS

A grant from the Fundamental Research Funds of the Central Universities of China was provided to conduct this research. The first author thanks the Shanghai Committee of Science and Technology (under Grant No. 23ZR1467800), Shanghai Sailing Program (under Grant No. 22YF1450100) and the State Key Laboratory of Marine Geology (under Grant No. MGZ202303) for their financial support. We thank Geoscience Australia for providing valuable seismic and multibeam bathymetry for the Gippsland Basin. We also thank Prof. Guangfa Zhong and Wei Li, Dr. Chao Liang for their supportive suggestions that enrich this work.

FIGURE CAPTIONS

Figure 1. (A) Regional map of Australia, showing the location of the study area and the oceanographic setting. BCC, Bass Cascade Current; EAC, East Australian Current. The dashed yellow polygon indicates the location of Figure 1B, the solid black polygon indicates the location of Figure 1C. (B) Seawater temperature map monitored on 14th January, 2020, highlighting the pathway of the EAC and its associated eddies. Figure 1B is modified from the Integrated Marine Observing System (IMOS) of Australia (http://oceancurrent.imos.org.au/index.php). (C) Zoom in view of the Gippsland Basin and the Bass Canyon. The pathway of the BCC is adopted from Tomczak (1985) and Tomczak (1987). The pathway of the EAC is adopted from Lavering (1994) and Ridgway and Hill (2009). The regional faults were modified after Hill et al. (1998) and O'Brien et al. (2018).

Figure 2. (A) Overview of hill-shaded seabed bathymetry map with contours (white dotted line) depicting the main morphologic features in the study area and the north-arrow (white). (B) Seabed slope gradient map with interpretations, showing the key depositional elements, major canyon names, and location of 3D seismic datasets.

Figure 3. (A) Shelf to Slope profile showing the upper-, middle- and lower part of the Northern slope. (B) Shelf to Slope profile depicting the upper-, middle- and lower part of the western Northern region. (C) Shelf-to-slope profile traversing across the Central shelf and slope regions. (D) Shelf to Slope profile illustrating the upper-, middle- and

lower part of the Southern region. See Figure 2B for locations.

Figure 4. (A) Multibeam bathymetric map (in slope gradient) in the Northern region. (B) Seismic section across the Northern slope. (C) Bathymetric profile cut across the gullies developed on the Northern slope. (D) Bathymetric profile extracted from the long axis of Everard Canyon. (E) Cross-sectional bathymetric profile cutting across the canyons in the lower slope area of the Northern region. See Figure 4A for locations.

Figure 5. (A) Seabed structure map of the Northern shelf calculated from 3D seismic data. (B) Seismic dip section cutting along the scarps developed on the shelf. (C) Seismic dip section cutting along the scarps developed on the shelf. See Figure 5A for locations.

Figure 6. (A) Seabed bathymetric map calculated from 3D seismic data, showing the seabed morphology in the Central region. (B) Seismic section cutting along the headwall scarp and cyclic scours developed on the shelf. (C) Seismic section cutting along the headwall scarp and cyclic step train developed on the shelf. (D) Seismic section cutting across the cyclic step train and channels developed on the shelf. (E) Seismic section cutting across the gullies that developed on the slope. See the location in Figure 6A.

Figure 7. (A) Multibeam bathymetric map (in slope gradient) showing the

interpretations of the seabed morphologies in the Southern region. (B) Bathymetric profile cutting across the upper section of the canyons in the Southern shelf. (C) Bathymetric profile cutting across the middle section of the canyons in the Southern slope. (D) Bathymetric profile cutting across the lower section of the canyons in the Southern slope. See Figure 7A for locations.

Figure 8. (A) Multibeam bathymetric map (in slope gradient) shows the zoomed-in profile of the Southern shelf with interpretations of the seabed morphologies. See Figure 7A for location. (B) Along-slope bathymetric profile cut through cyclic steps developed on the shelf. (C) Bathymetric profile cut across the gullies and Pisces Canyon, showing their cross-sectional profiles. (D) Bathymetric profile cut along cyclic steps developed on the upper slope. See the location in Figure 8A.

Figure 9. (A) Multibeam bathymetric map (in slope gradient) shows the zoomed-in profile of the lower slope with interpretations of the seabed morphologies. See Figure 7A for location. (B) Bathymetric profile cut along cyclic steps developed on the lower slope. (C) Bathymetric profile cut across the canyon on the lower slope. See the location in Figure 9A.

Figure 10. (A) Sketch showing the time-step process of retrogressive canyon evolution. (B) Sketch showing the downslope, time-step channel evolution processes. Figure 10B is adopted from Fildani et al. (2013).

Table 1. 3D seismic reflection data and their properties used in the study.

Seismic data	Vintage	Water Depth (m)	Area (km^2)	Bin Size (m)		Frequency （Seabed）	Vertical Resolution (m)
				Xline	Inline		
Elver 3D	2007	150-2700	650	25	25	40	12.5
Tuskfish 3D	2004	150-2700	1050	12.5	18.75	50	10
Oscar 3D	2006	800-1500	1200	25	18.75	40	12.5

REFERENCE

Hocking, J. B., 1972, Geologic evolution and hydrocarbon habitat Gippsland Basin: The APPEA Journal, v. 12, no. 1, p. 132-137.

Marshall, N., Stanley, D., and Kelling, G., 1978, Large storm-induced sediment slump reopens an unknown Scripps submarine canyon tributary: Sedimentation in submarine canyons, fans, and trenches: Stroudsburg, Pennsylvania, Hutchinson and Ross, p. 73-84.

Godfrey, J., Jones, I., Maxwell, G., and Scott, B., 1980, On the winter cascade from Bass Strait into the Tasman Sea: Marine and Freshwater Research, v. 31, no. 3, p. 275-286.

Boland, F., and Church, J., 1981, The east Australian current 1978: Deep Sea Research Part A. Oceanographic Research Papers, v. 28, no. 9, p. 937-957.

Bea, R. G., Wright, S. G., Sircar, P., and Niedoroda, A. W., 1983, Wave-induced slides in south pass block 70, Mississippi Delta: Journal of Geotechnical Engineering, v. 109, no. 4, p. 619-644.

Farre, J. A., McGregor, B. A., Ryan, W. B., and Robb, J. M., 1983, Breaching the shelfbreak: passage from youthful to mature phase in submarine canyon evolution.

Hegarty, K., Duddy, I., Green, P., Gleadow, A., Fraser, I., and Weissel, J., 1985, Regional evaluation of the tectonic and thermal history of the Gippsland Basin.

Tomczak, 1985, The Bass Strait water cascade during winter 1981: Continental Shelf Research, v. 4, no. 3, p. 255-278.

Godfrey, J., Vaudrey, D., and Hahn, S., 1986, Observations of the shelf-edge current south of Australia, winter 1982: Journal of Physical Oceanography, v. 16, no. 4, p. 668-679.

Tomczak, M., 1987, The Bass Strait water cascade during summer 1981–1982: Continental Shelf Research, v. 7, no. 6, p. 561-572.

Flood, R. D., 1988, A lee wave model for deep-sea mudwave activity: Deep Sea Research Part A. Oceanographic Research Papers, v. 35, no. 6, p. 973-983.

Blumsack, S., and Weatherly, G., 1989, Observations of the nearby flow and a model for the growth of mudwaves: Deep Sea Research Part A. Oceanographic Research Papers, v. 36, no. 9, p. 1327-1339.

Rahmanian, V., Moore, P., Mudge, W., and Spring, D., 1990, Sequence stratigraphy and the habitat of hydrocarbons, Gippsland Basin, Australia: Geological Society, London, Special Publications, v. 50, no. 1, p. 525-544.

Willcox, J., Colwell, J., and Constantine, A., 1992, New ideas on Gippsland Basin regional tectonics.

Colwell, J. B., Constantine, A. E., and Willcox, J. B., 1993, Regional structure of the Gippsland Basin: interpretation and mapping of a deep seismic data set, Australian Geological Survey Organisation.

Howe, J., Stoker, M., and Stow, D., 1994, Late Cenozoic sediment drift complex, northeast Rockall trough, North Atlantic: Paleoceanography, v. 9, no. 6, p. 989-999.

Lavering, I. H., 1994, Marine environments of Southeast Australia (Gippsland Shelf and Bass Strait) and the impact of offshore petroleum exploration and production activity: Marine georesources & geotechnology, v. 12, no. 3, p. 201-226.

Pratson, L. F., and Coakley, B. J., 1996, A model for the headward erosion of submarine canyons induced by downslope-eroding sediment flows: Geological Society of America Bulletin, v. 108, no. 2, p. 225-234.

Bryant, E. A., and Price, D., 1997, Late Pleistocene marine chronology of the Gippsland Lakes region, Australia: Physical Geography, v. 18, no. 4, p. 318-334.

Hill, P., Exon, N., Keene, J., and Smith, S., 1998, The continental margin off east Tasmania and Gippsland: structure and development using new multibeam sonar data: Exploration

Geophysics, v. 29, no. 4, p. 410-419.

Faugères, J.-C., Stow, D. A., Imbert, P., and Viana, A., 1999, Seismic features diagnostic of contourite drifts: Marine Geology, v. 162, no. 1, p. 1-38.

Gardner, J. V., Prior, D. B., and Field, M. E., 1999, Humboldt slide—a large shear-dominated retrogressive slope failure: Marine Geology, v. 154, no. 1-4, p. 323-338.

Paull, C., Ussler, W., Greene, H., Keaten, R., Mitts, P., and Barry, J., 2002, Caught in the act: the 20 December 2001 gravity flow event in Monterey Canyon: Geo-Marine Letters, v. 22, no. 4, p. 227-232.

Stow, D. A., Faugères, J.-C., Howe, J. A., Pudsey, C. J., and Viana, A. R., 2002, Bottom currents, contourites and deep-sea sediment drifts: current state-of-the-art: Geological Society, London, Memoirs, v. 22, no. 1, p. 7-20.

Fildani, A., and Normark, W. R., 2004, Late Quaternary evolution of channel and lobe complexes of Monterey Fan: Marine Geology, v. 206, no. 1-4, p. 199-223.

Ivanov, V., Shapiro, G., Huthnance, J., Aleynik, D., and Golovin, P., 2004, Cascades of dense water around the world ocean: Progress in oceanography, v. 60, no. 1, p. 47-98.

Krassay, A., Cathro, D., and Ryan, D., 2004, A regional tectonostratigraphic framework for the Otway Basin.

Bryn, P., Berg, K., Forsberg, C. F., Solheim, A., and Kvalstad, T. J., 2005, Explaining the Storegga slide: Marine and Petroleum Geology, v. 22, no. 1, p. 11-19.

Li, F., Dyt, C., Griffiths, C., Jenkins, C., Rutherford, M., and Chittleborough, J., 2005, Seabed sediment transport and offshore pipeline risks in the Australian southeast: The APPEA Journal, v. 45, no. 1, p. 523-534.

Solheim, A., Berg, K., Forsberg, C., and Bryn, P., 2005, The Storegga Slide complex: repetitive large scale sliding with similar cause and development: Marine and Petroleum Geology, v. 22, no. 1-2, p. 97-107.

Fildani, A., Normark, W. R., Kostic, S., and Parker, G., 2006, Channel formation by flow stripping: Large‐scale scour features along the Monterey East Channel and their relation to sediment waves: Sedimentology, v. 53, no. 6, p. 1265-1287.

Mitchell, J., Holdgate, G., and Wallace, M., 2007a, Pliocene–Pleistocene history of the Gippsland Basin outer shelf and canyon heads, southeast Australia: Australian Journal of Earth Sciences, v. 54, no. 1, p. 49-64.

Mitchell, J., Holdgate, G., Wallace, M., and Gallagher, S., 2007b, Marine geology of the Quaternary Bass Canyon system, southeast Australia: a cool-water carbonate system: Marine geology, v. 237, no. 1-2, p. 71-96.

Laberg, J., and Camerlenghi, A., 2008, The significance of contourites for submarine slope stability: Developments in sedimentology, v. 60, p. 537-556.

Bull, S., Cartwright, J., and Huuse, M., 2009, A review of kinematic indicators from mass-transport complexes using 3D seismic data: Marine and Petroleum Geology, v. 26, no. 7, p. 1132-1151.

Canals, M., Danovaro, R., Heussner, S., Lykousis, V., Puig, P., Trincardi, F., Calafat, A. M., de Madron, X. D., Palanques, A., and Sanchez-Vidal, A., 2009, Cascades in Mediterranean submarine grand canyons: Oceanography, v. 22, no. 1, p. 26-43.

Hsu, S., Tsai, C., Ku, C., and Sibuet, J., Flow of turbidity currents as evidenced by failure of submarine telecommunication cables, *in* Proceedings International Conference on Seafloor Mapping for Geohazard Assessment, Extended Abstracts, Rendiconti online, Società Geologica Italiana2009, Volume 7, p. 167-171.

Noormets, R., Dowdeswell, J., Larter, R. D., Cofaigh, C. Ó., and Evans, J., 2009, Morphology of the upper continental slope in the Bellingshausen and Amundsen Seas–Implications for sedimentary processes at the shelf edge of West Antarctica: Marine Geology, v. 258, no. 1-4, p. 100-114.

Normark, W. R., Paull, C. K., Caress, D. W., USSLER III, W., and Sliter, R., 2009, Fine‐scale relief related to Late Holocene channel shifting within the floor of the upper Redondo Fan, offshore Southern California: Sedimentology, v. 56, no. 6, p. 1690-1704.

Ridgway, K., and Hill, K., 2009, The East Australian Current.

Sawyer, D. E., Flemings, P. B., Dugan, B., and Germaine, J. T., 2009, Retrogressive failures recorded in mass transport deposits in the Ursa Basin, Northern Gulf of Mexico: Journal of Geophysical Research: Solid Earth, v. 114, no. B10.

Jobe, Z. R., Lowe, D. R., and Uchytil, S. J., 2011, Two fundamentally different types of submarine canyons along the continental margin of Equatorial Guinea: Marine and Petroleum Geology, v. 28, no. 3, p. 843-860.

Kostic, S., 2011, Modeling of submarine cyclic steps: Controls on their formation, migration, and architecture: Geosphere, v. 7, no. 2, p. 294-304.

Micallef, A., and Mountjoy, J. J., 2011, A topographic signature of a hydrodynamic origin for submarine gullies: Geology, v. 39, no. 2, p. 115-118.

Suthers, I. M., Young, J. W., Baird, M. E., Roughan, M., Everett, J. D., Brassington, G. B., Byrne, M., Condie, S. A., Hartog, J. R., and Hassler, C. S., 2011, The strengthening East Australian Current, its eddies and biological effects—an introduction and overview, Volume 58, Elsevier, p. 538-546.

Gales, J., Larter, R., Mitchell, N., Hillenbrand, C. D., Østerhus, S., and Shoosmith, D., 2012, Southern Weddell Sea shelf edge geomorphology: Implications for gully formation by the overflow of high‐salinity water: Journal of Geophysical Research: Earth Surface, v. 117, no. F4.

Fildani, A., Hubbard, S. M., Covault, J. A., Maier, K. L., Romans, B. W., Traer, M., and Rowland, J. C., 2013, Erosion at inception of deep-sea channels: Marine and Petroleum Geology, v. 41, p. 48-61.

Lonergan, L., Jamin, N. H., Jackson, C. A.-L., and Johnson, H. D., 2013, U-shaped slope gully systems and sediment waves on the passive margin of Gabon (West Africa): Marine Geology, v. 337, p. 80-97.

Puga-Bernabéu, Á., Webster, J. M., Beaman, R. J., and Guilbaud, V., 2013, Variation in canyon morphology on the Great Barrier Reef margin, north-eastern Australia: The influence of slope and barrier reefs: Geomorphology, v. 191, p. 35-50.

Carter, L., Gavey, R., Talling, P. J., and Liu, J. T., 2014, Insights into submarine geohazards from breaks in subsea telecommunication cables: Oceanography, v. 27, no. 2, p. 58-67.

He, Y., Zhong, G., Wang, L., and Kuang, Z., 2014, Characteristics and occurrence of submarine canyon-associated landslides in the middle of the northern continental slope, South China Sea: Marine and Petroleum Geology, v. 57, p. 546-560.

Parsons, T., Geist, E. L., Ryan, H. F., Lee, H. J., Haeussler, P. J., Lynett, P., Hart, P. E., Sliter, R., and Roland, E., 2014, Source and progression of a submarine landslide and tsunami: The 1964 Great Alaska earthquake at Valdez: Journal of Geophysical Research: Solid Earth, v. 119, no. 11, p. 8502-8516.

Zhong, G., Cartigny, M. J., Kuang, Z., and Wang, L., 2015, Cyclic steps along the South Taiwan Shoal and West Penghu submarine canyons on the northeastern continental slope of the South China Sea: Bulletin, v. 127, no. 5-6, p. 804-824.

Miramontes, E., Cattaneo, A., Jouet, G., Thereau, E., Thomas, Y., Rovere, M., Cauquil, E., and Trincardi, F., 2016, The Pianosa contourite depositional system (northern Tyrrhenian Sea): Drift morphology and Plio-Quaternary stratigraphic evolution: Marine Geology, v. 378, p. 20-42.

Rashid, H., MacKillop, K., Sherwin, J., Piper, D., Marche, B., and Vermooten, M., 2017, Slope instability on a shallow contourite-dominated continental margin, southeastern Grand Banks, eastern Canada: Marine Geology, v. 393, p. 203-215.

Miramontes, E., Garziglia, S., Sultan, N., Jouet, G., and Cattaneo, A., 2018, Morphological control of slope instability in contourites: a geotechnical approach: Landslides, v. 15, no. 6, p. 1085-1095.

O'Brien, P., Mitchell, C., Nguyen, D., and Langford, R., 2018, Mass Transport Complexes on a Cenozoic paleo-shelf edge, Gippsland basin, southeastern Australia: Marine and Petroleum Geology, v. 98, p. 783-801.

Yin, S., Lin, L., Pope, E. L., Li, J., Ding, W., Wu, Z., Ding, W., Gao, J., and Zhao, D., 2019, Continental slope-confined canyons in the Pearl River Mouth Basin in the South China Sea dominated by erosion, 2004–2018: Geomorphology, v. 344, p. 60-74.

Brackenridge, R. E., Nicholson, U., Sapiie, B., Stow, D., and Tappin, D. R., 2020, Indonesian Throughflow as a preconditioning mechanism for submarine landslides in the Makassar Strait: Geological Society, London, Special Publications, v. 500, no. 1, p. 195-217.

De Castro, S., Hernández-Molina, F., Rodríguez-Tovar, F., Llave, E., Ng, Z., Nishida, N., and Mena, A., 2020, Contourites and bottom current reworked sands: Bed facies model and implications: Marine Geology, v. 428, p. 106267.

Gardner, J. V., Peakall, J., Armstrong, A. A., and Calder, B. R., 2020, The Geomorphology of Submarine Channel Systems of the Northern Line Islands Ridge, Central Equatorial Pacific Ocean: Frontiers in Earth Science, v. 8, p. 87.

Gatter, R., Clare, M. A., Hunt, J. E., Watts, M., Madhusudhan, B., Talling, P. J., and Huhn, K., 2020, A multi-disciplinary investigation of the AFEN Slide: the relationship between contourites and submarine landslides: Geological Society, London, Special Publications, v. 500, no. 1, p. 173-193.

Morrison, A., Hogg, A. M., England, M. H., and Spence, P., 2020, Warm Circumpolar Deep Water transport toward Antarctica driven by local dense water export in canyons: Science advances, v. 6, no. 18, p. eaav2516.

Nicholson, U., Libby, S., Tappin, D. R., and McCarthy, D., 2020, The Subantarctic Front as a sedimentary conveyor belt for tsunamigenic submarine landslides: Marine Geology, v. 424, p. 106161.

Miramontes, E., Thiéblemont, A., Babonneau, N., Penven, P., Raisson, F., Droz, L., Jorry, S. J., Fierens, R., Counts, J. W., and Wilckens, H., 2021, Contourite and mixed turbidite-contourite systems in the Mozambique Channel (SW Indian Ocean): Link between geometry, sediment characteristics and modelled bottom currents: Marine Geology, v. 437, p. 106502.

Wu, N., Nugraha, H. D., Zhong, F. G., and Steventon, M., 2021, The role of mass-transport complexes (MTCs) in the initiation and evolution of submarine canyons.

Post, A. L., Przeslawski, R., Nanson, R., Siwabessy, J., Smith, D., Kirkendale, L. A., and Wilson, N. G., 2022, Modern dynamics, morphology and habitats of slope-confined canyons on the northwest Australian margin: Marine Geology, v. 443, p. 106694.

Wu, N., Nugraha, H. D., Zhong, G., and Steventon, M. J., 2022, The role of mass-transport complexes in the initiation and evolution of submarine canyons: Sedimentology.

Wu, N., Zhong, F. G., Niyazi, Y., Nugraha, H. D., and Steventon, M., 2023, Transformation of dense shelf water cascade to supercritical turbidity currents: Impact on seabed geomorphology and implication for climate change.

Figure 1

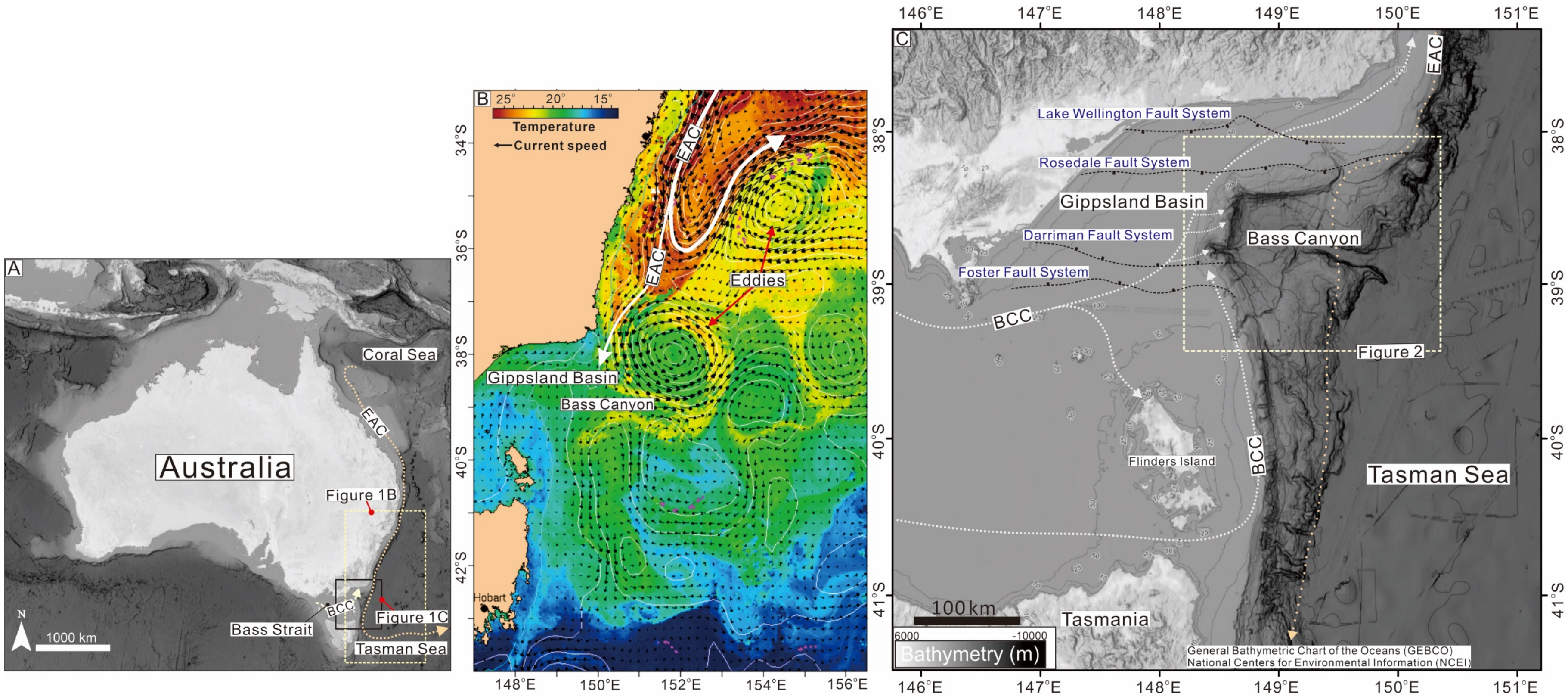
A
Coral Sea
EAC
Australia
Figure 1B
BCC
Bass Strait
Figure 1C
Tasman Sea
N
1000 km
B
25° 20° 15°
Temperature
Current speed
EAC
EAC
Eddies
Gippsland Basin
Bass Canyon
Hobart
34°S
36°S
38°S
40°S
42°S
148°E 150°E 152°E 154°E 156°E
C
146°E 147°E 148°E 149°E 150°E 151°E
EAC
Lake Wellington Fault System
Rosedale Fault System
Gippsland Basin
Darriman Fault System
Bass Canyon
Foster Fault System
BCC
Figure 2
Flinders Island
BCC
Tasman Sea
100 km
Tasmania
6000 -10000
Bathymetry (m)
General Bathymetric Chart of the Oceans (GEBCO)
National Centers for Environmental Information (NCEI)
38°S
39°S
40°S
41°S

Figure 2

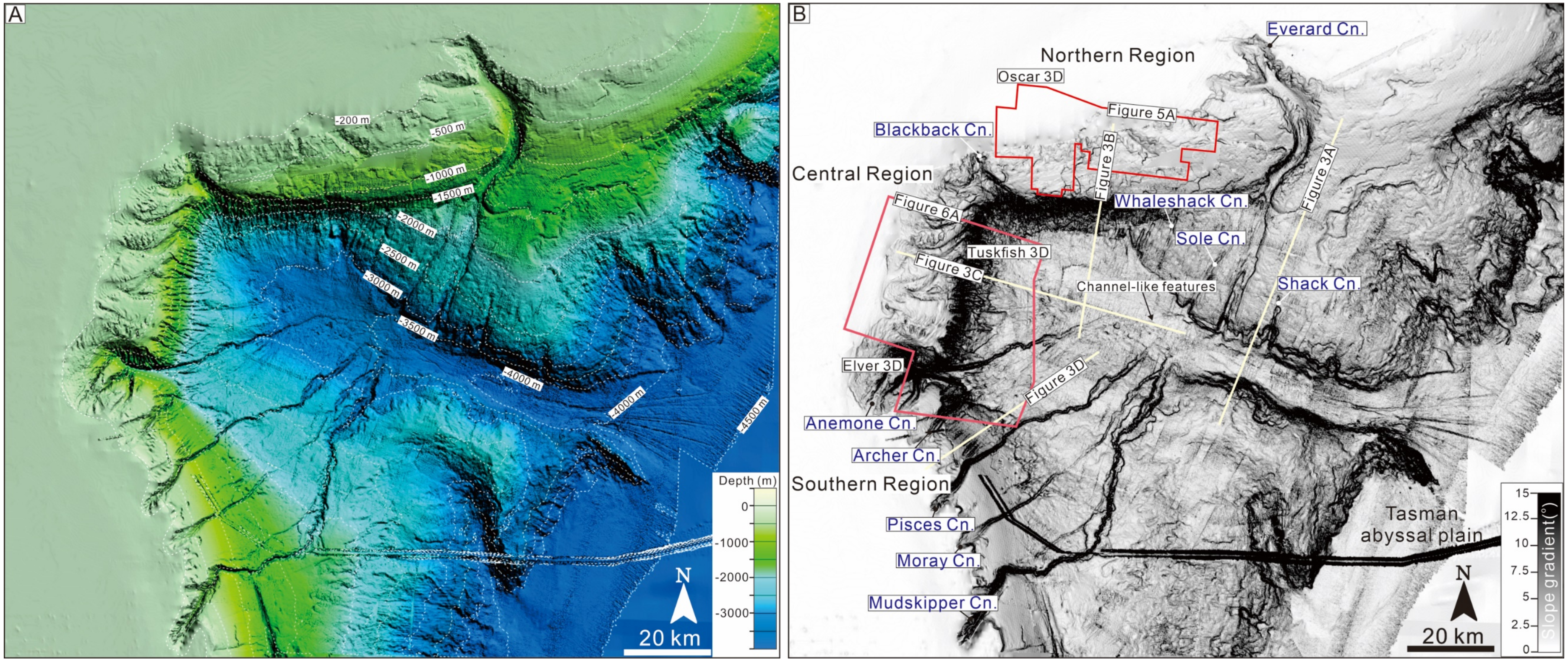

A
-200 m
-500 m
-1000 m
-1500 m
-2000 m
-2500 m
-3000 m
-3500 m
-4000 m
-4000 m
-4500 m
Depth (m)
0
-1000
-2000
-3000
N
20 km
B
Everard Cn.
Northern Region
Oscar 3D
Figure 5A
Blackback Cn.
Figure 3B
Figure 3A
Central Region
Whaleshack Cn.
Figure 6A
Sole Cn.
Tuskfish 3D
Figure 3C
Channel-like features
Shack Cn.
Elver 3D
Figure 3D
Anemone Cn.
Archer Cn.
Southern Region
Pisces Cn.
Moray Cn.
Mudskipper Cn.
Tasman abyssal plain
N
20 km
15
12.5
10
7.5
5
2.5
0
Slope gradient(°)

Figure 3

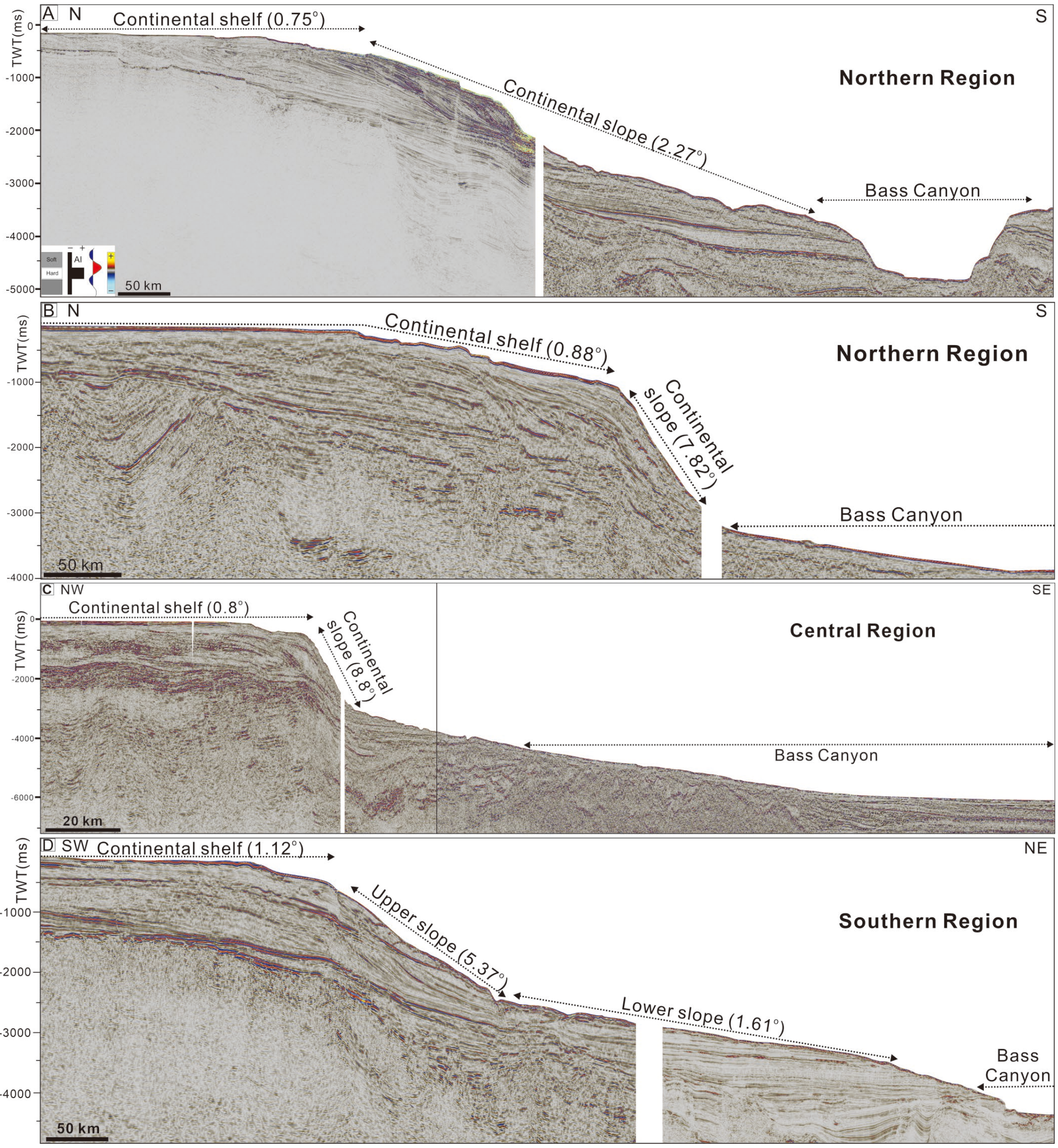

A N
Continental shelf (0.75°)
S
Northern Region
Continental slope (2.27°)
Bass Canyon
TWT (ms)
0
-1000
-2000
-3000
-4000
-5000
Soft
Hard
AI
50 km
B N
Continental shelf (0.88°)
S
Northern Region
Continental slope (7.82°)
Bass Canyon
-1000
-2000
-3000
-4000
50 km
C NW
Continental shelf (0.8°)
Continental slope (8.8°)
SE
Central Region
Bass Canyon
0
-2000
-4000
-6000
20 km
D SW
Continental shelf (1.12°)
NE
Upper slope (5.37°)
Southern Region
Lower slope (1.61°)
Bass Canyon
-1000
-2000
-3000
-4000
50 km

Figure 4

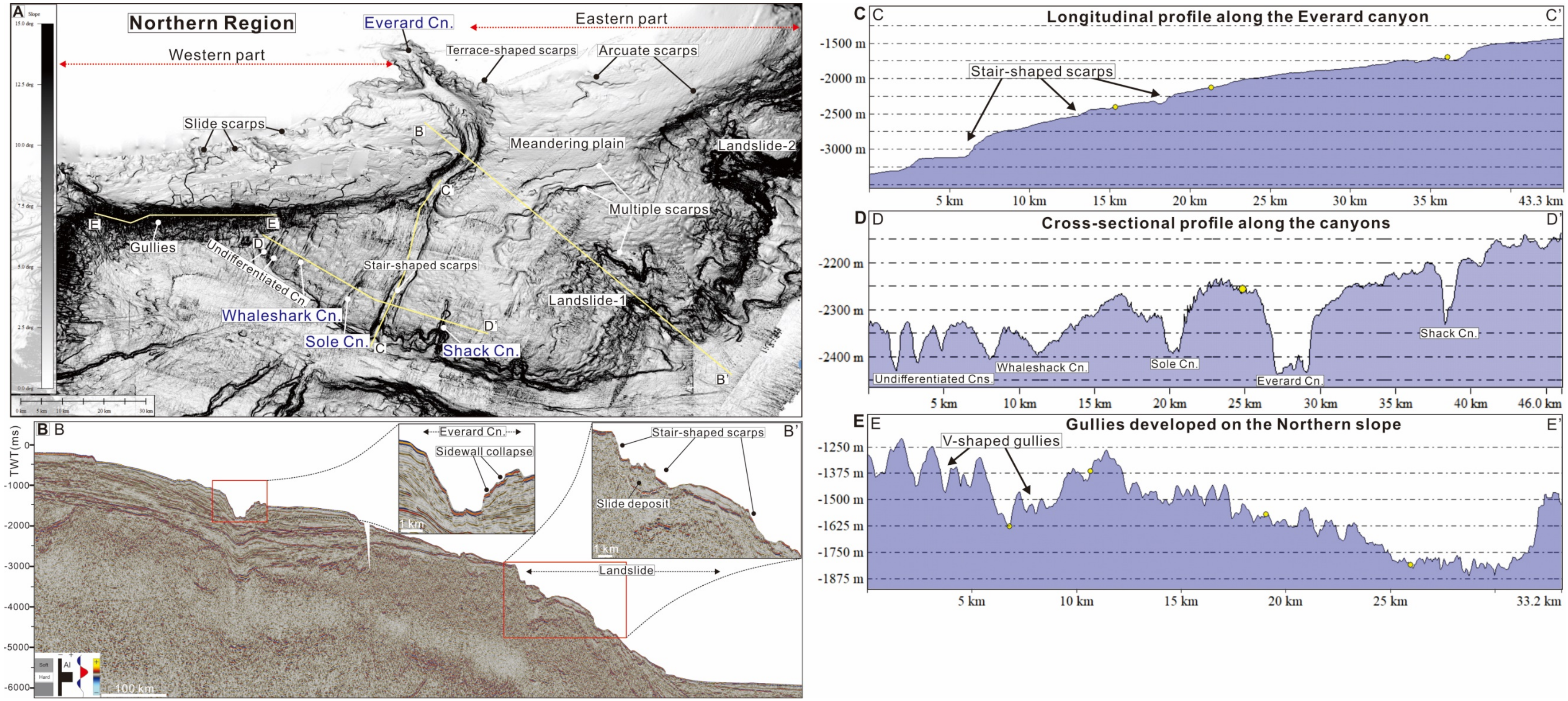

A
Northern Region
Everard Cn.
Eastern part
Western part
Terrace-shaped scarps
Arcuate scarps
Slide scarps
Meandering plain
Landslide-2
Multiple scarps
Gullies
Undifferentiated Cn.
Stair-shaped scarps
Whaleshark Cn.
Landslide-1
Sole Cn.
Shack Cn.
B
TWT(ms)
Everard Cn.
Sidewall collapse
Stair-shaped scarps
Slide deposit
Landslide
100 km
C
Longitudinal profile along the Everard canyon
Stair-shaped scarps
D
Cross-sectional profile along the canyons
Undifferentiated Cns
Whaleshack Cn.
Sole Cn.
Everard Cn.
Shack Cn.
E
Gullies developed on the Northern slope
V-shaped gullies

Figure 5

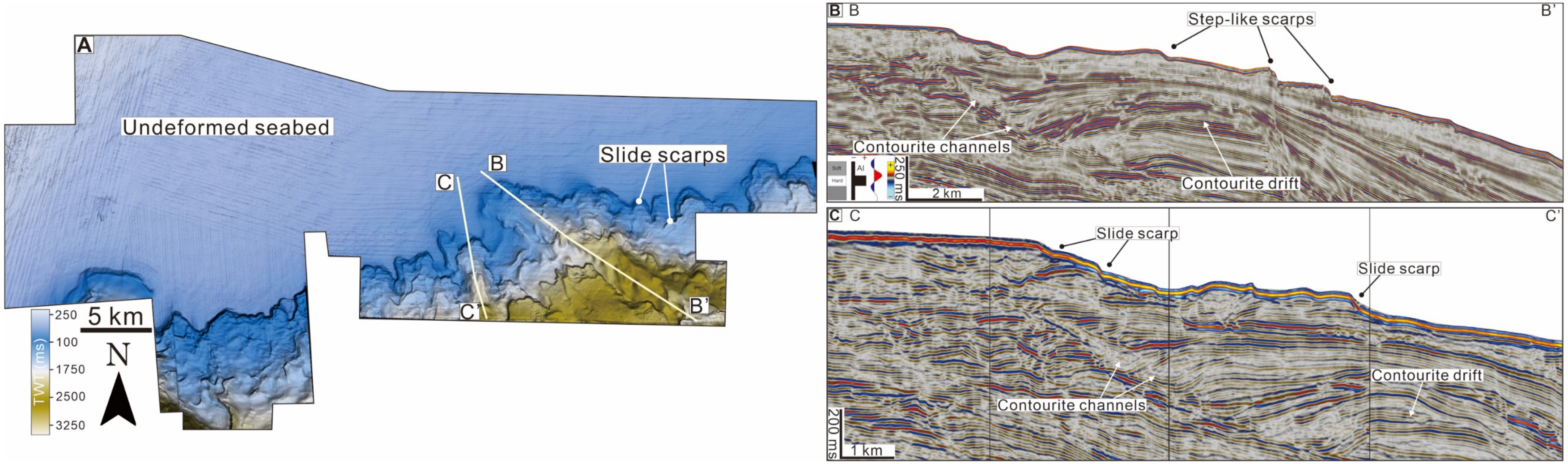

A
Undeformed seabed
Slide scarps
B
C
C'
B'
5 km
N
TWT (ms)
250
100
1750
2500
3250
B
B
B'
Step-like scarps
Contourite channels
Contourite drift
250 ms
2 km
C
C
C'
Slide scarp
Slide scarp
Contourite channels
Contourite drift
200 ms
1 km

Figure 6

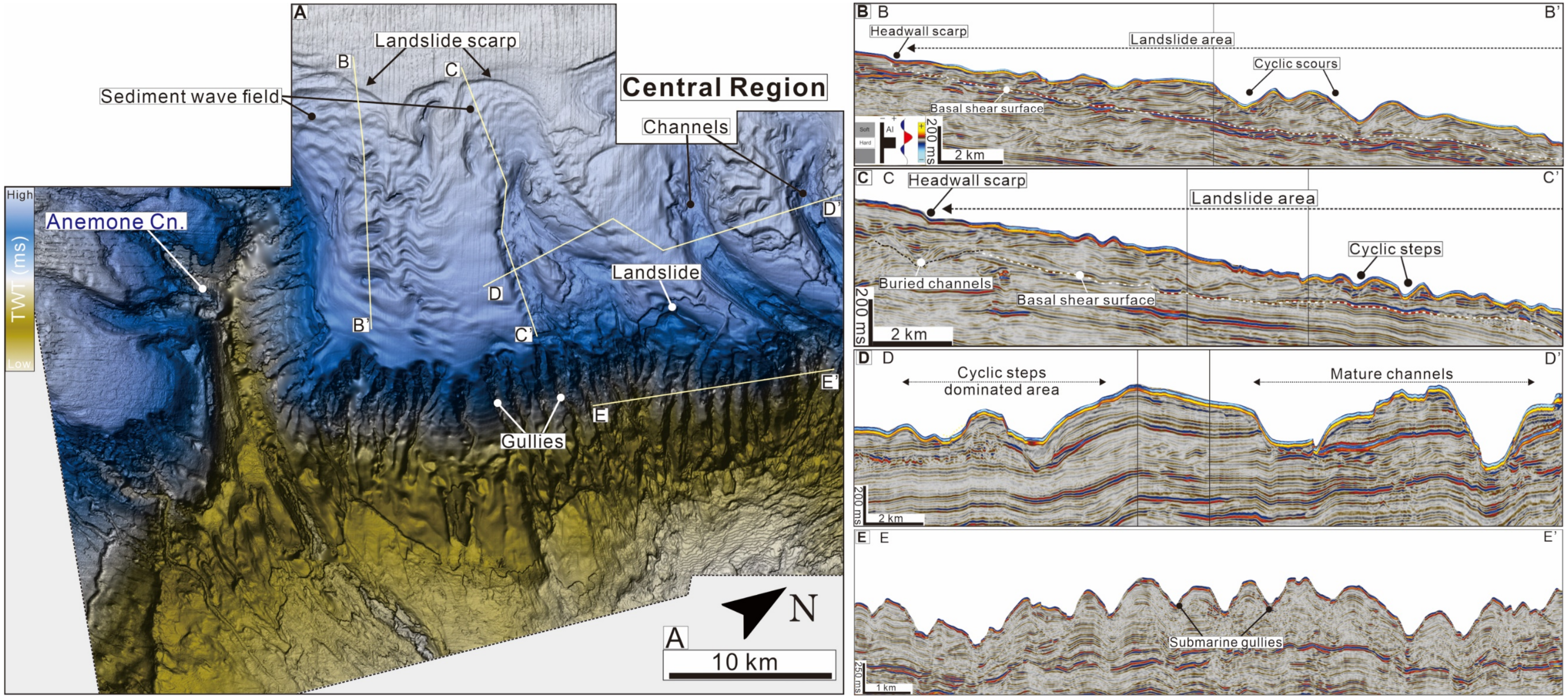
A
Landslide scarp
B
C
Sediment wave field
Central Region
Channels
D'
High
TWT (ms)
Low
Anemone Cn.
Landslide
D
B'
C'
E'
E
Gullies
N
A
10 km
B B
B'
Headwall scarp
Landslide area
Cyclic scours
Basal shear surface
200 ms
2 km
C C
C'
Headwall scarp
Landslide area
Cyclic steps
Buried channels
Basal shear surface
200 ms
2 km
D D
D'
Cyclic steps
dominated area
Mature channels
200 ms
2 km
E E
E'
Submarine gullies
250 ms
1 km

Figure 7

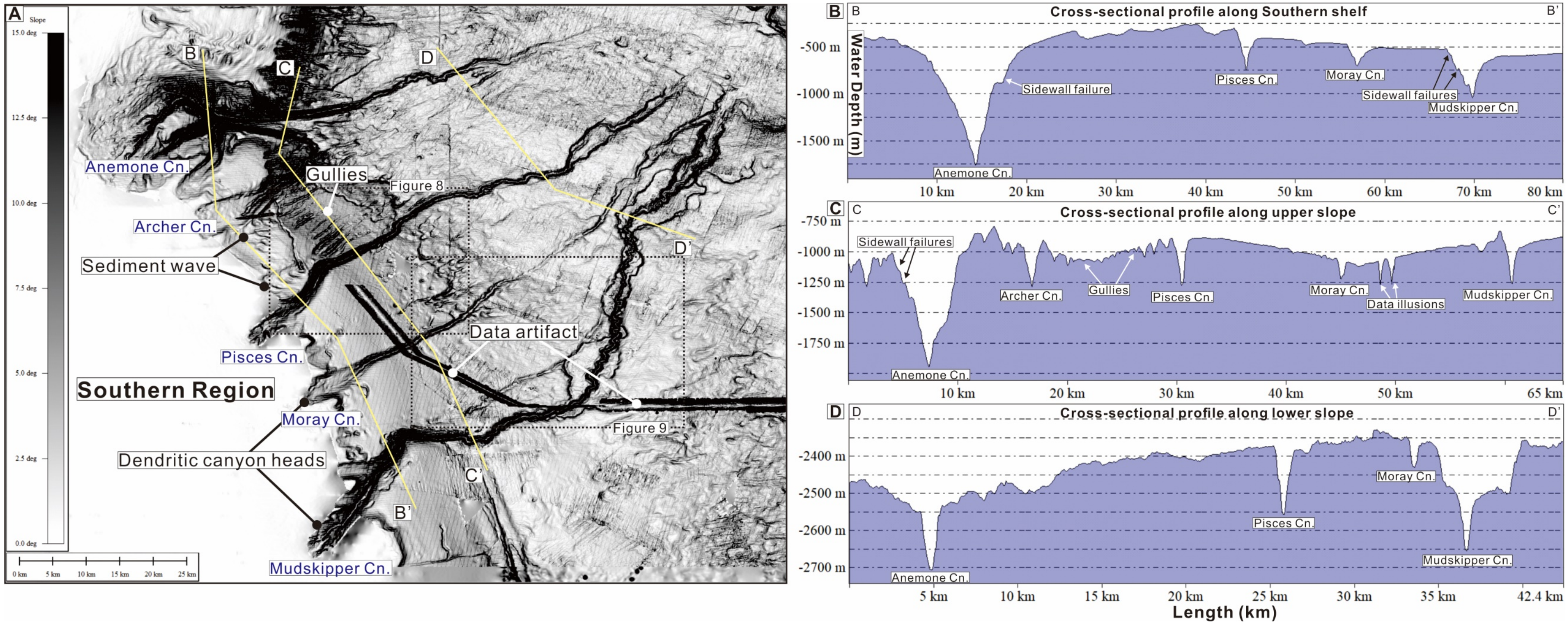

A
Slope
15.0 deg
12.5 deg
10.0 deg
7.5 deg
5.0 deg
2.5 deg
0.0 deg
0 km
5 km
10 km
15 km
20 km
25 km
B
C
D
Anemone Cn.
Gullies
Figure 8
Archer Cn.
Sediment wave
D'
Data artifact
Pisces Cn.
Southern Region
Moray Cn.
Figure 9
Dendritic canyon heads
C'
B'
Mudskipper Cn.
B
Cross-sectional profile along Southern shelf
Water Depth (m)
-500 m
-1000 m
-1500 m
Sidewall failure
Pisces Cn.
Moray Cn.
Sidewall failures
Mudskipper Cn.
Anemone Cn.
10 km
20 km
30 km
40 km
50 km
60 km
70 km
80 km
C
Cross-sectional profile along upper slope
-750 m
-1000 m
-1250 m
-1500 m
-1750 m
Sidewall failures
Archer Cn.
Gullies
Pisces Cn.
Moray Cn.
Data illusions
Mudskipper Cn.
Anemone Cn.
10 km
20 km
30 km
40 km
50 km
65 km
D
Cross-sectional profile along lower slope
-2400 m
-2500 m
-2600 m
-2700 m
Moray Cn.
Pisces Cn.
Mudskipper Cn.
Anemone Cn.
5 km
10 km
15 km
20 km
25 km
30 km
35 km
42.4 km
Length (km)

Figure 8

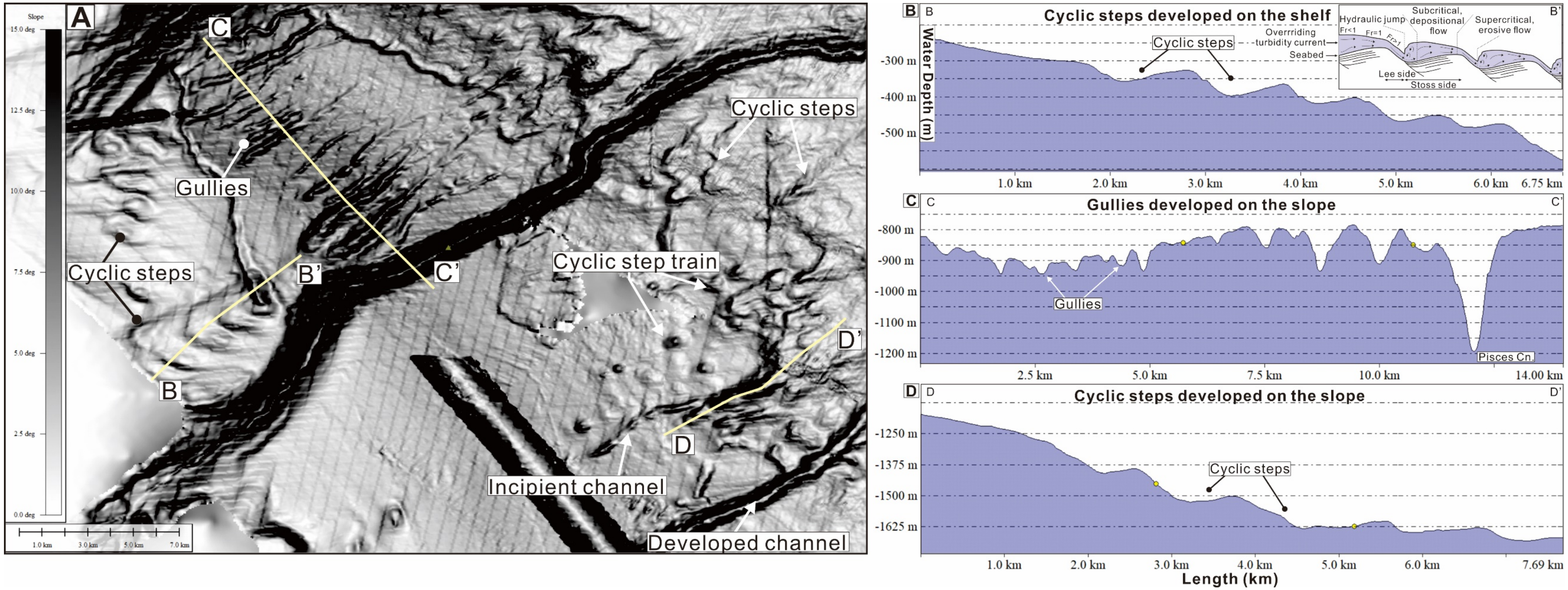
A
B
C
D
Slope
15.0 deg
12.5 deg
10.0 deg
7.5 deg
5.0 deg
2.5 deg
0.0 deg
1.0 km
3.0 km
5.0 km
7.0 km
C
C'
B
B'
D
D'
Gullies
Cyclic steps
Cyclic steps
Cyclic step train
Incipient channel
Developed channel
Cyclic steps developed on the shelf
Water Depth (m)
-300 m
-400 m
-500 m
Cyclic steps
Hydraulic jump
Subcritical, depositional flow
Supercritical, erosive flow
Overrriding turbidity current
Seabed
Lee side
Stoss side
1.0 km
2.0 km
3.0 km
4.0 km
5.0 km
6.0 km
6.75 km
Gullies developed on the slope
-800 m
-900 m
-1000 m
-1100 m
-1200 m
Gullies
Pisces Cn
2.5 km
5.0 km
7.5 km
10.0 km
14.00 km
Cyclic steps developed on the slope
-1250 m
-1375 m
-1500 m
-1625 m
Cyclic steps
1.0 km
2.0 km
3.0 km
4.0 km
5.0 km
6.0 km
7.69 km
Length (km)

Figure 9

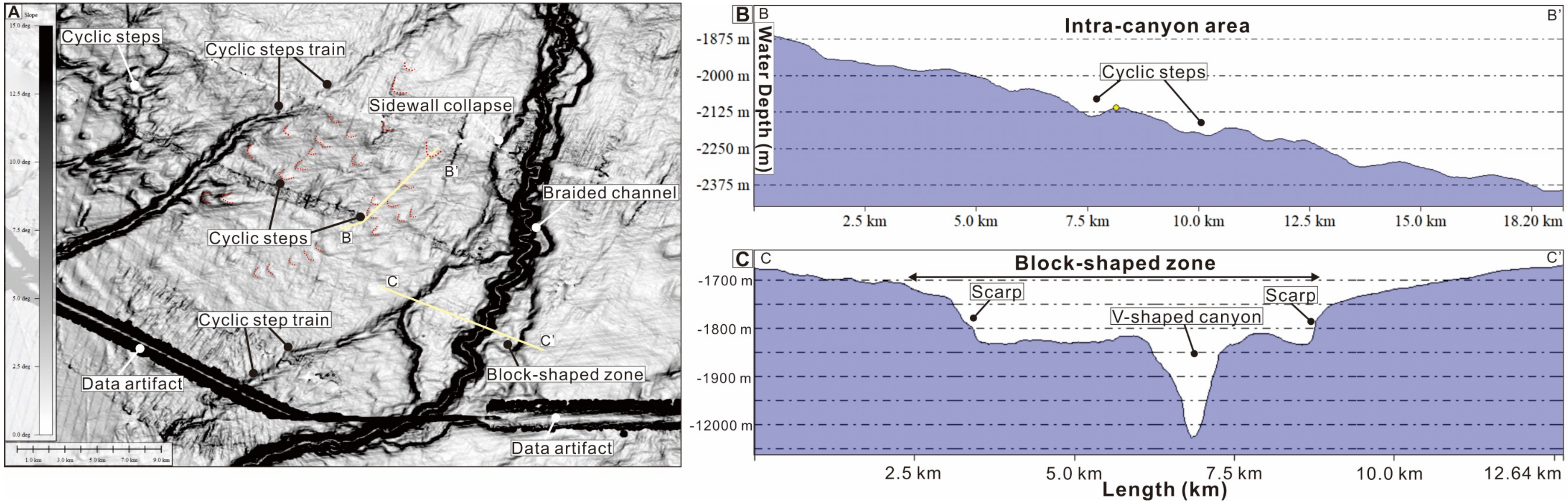

A
Cyclic steps
Cyclic steps train
Sidewall collapse
B'
Braided channel
Cyclic steps
B
C
Cyclic step train
C'
Data artifact
Block-shaped zone
Data artifact
B
Intra-canyon area
Cyclic steps
Water Depth (m)
-1875 m
-2000 m
-2125 m
-2250 m
-2375 m
2.5 km
5.0 km
7.5 km
10.0 km
12.5 km
15.0 km
18.20 km
C
Block-shaped zone
Scarp
Scarp
V-shaped canyon
-1700 m
-1800 m
-1900 m
-12000 m
2.5 km
5.0 km
7.5 km
10.0 km
12.64 km
Length (km)

Figure 10

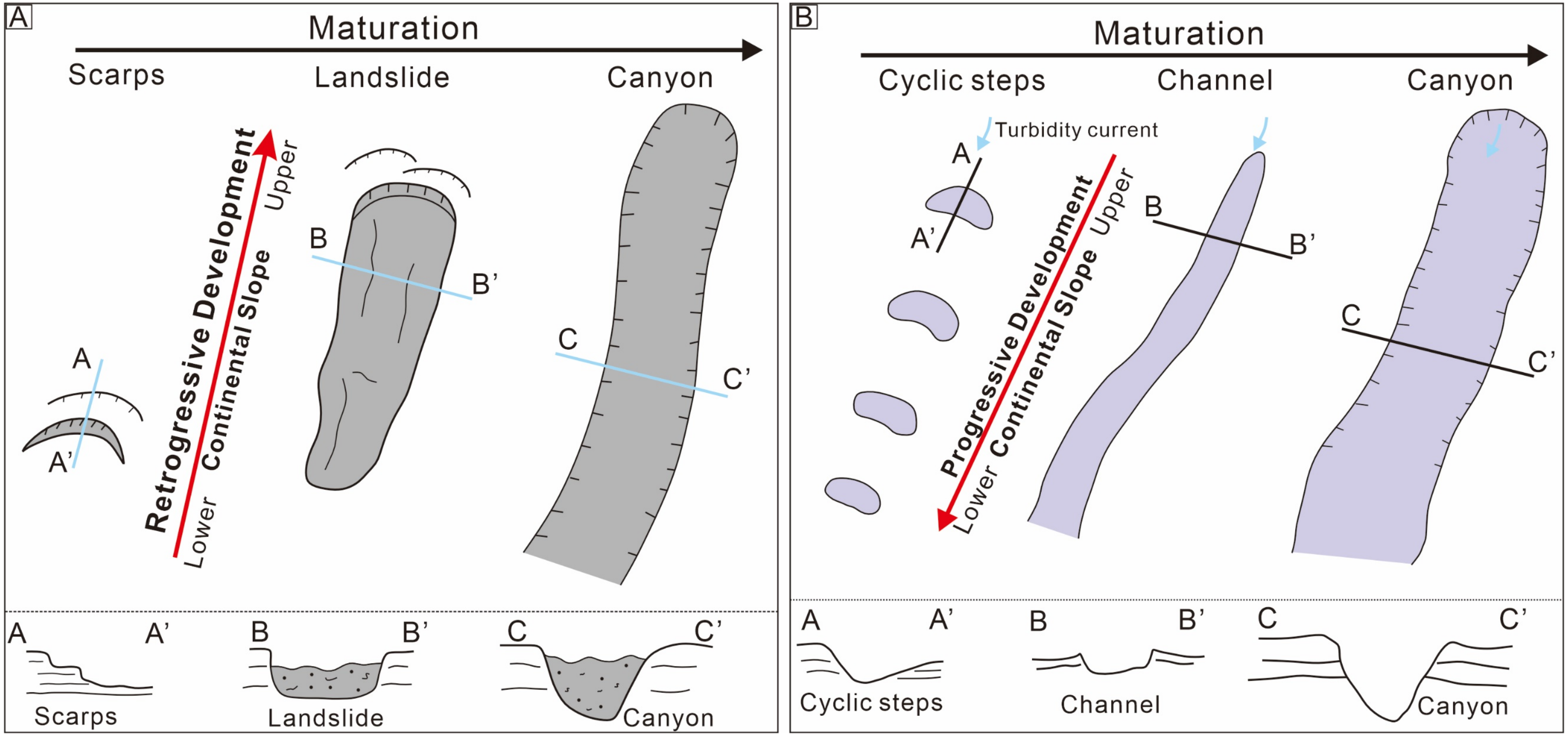

A
Maturation
Scarps
Landslide
Canyon
Retrogressive Development
Continental Slope
Upper
Lower
A
A'
B
B'
C
C'
A
A'
Scarps
B
B'
Landslide
C
C'
Canyon
B
Maturation
Cyclic steps
Channel
Canyon
Turbidity current
Progressive Development
Continental Slope
Upper
Lower
A
A'
B
B'
C
C'
A
A'
Cyclic steps
B
B'
Channel
C
C'
Canyon